International Journal of
INTELLIGENT SYSTEMS AND APPLICATIONS IN ENGINEERING
ISSN:2147-6799 www.ijisae.org Original Research Paper

An Optimized CNN GNR Detector for Methane Gas Detection from HSI Raster Data Using Feature Variable

Sneha G. Venkateshalu [1], Santhosh Laxman Deshpande *[2]

Submitted: 18/09/2023 **Revised**: 17/11/2023 **Accepted**: 29/11/2023

Abstract: Methane gas is the Earth's atmospheric second most significant greenhouse gas, so to reduce these emissions effective deep learning methods adopted. Methane source points and dimensions can be determined using airborne remote sensing AVIRIS-NG. The existing manual approaches, small pixel-footprint signal of the plumes causes them liable to human error and poorly scalable. The proposed Convolutional Neural Network (CNN) adapted from MATLAB toolbox to produce outcome of linear combinatorial pixel segmentation with accounting time. The target of the innovative is to segment the methane gas accurately considering minimization of the misclassification of plumes among terrain HSI raster data. Employing off-the-shelf CNN with available filters, the recursive filters applied to achieve long impulse response without having the reflectance to perform a long convolution. The SSIM metric evaluated the accuracy and the proposed approach produced outcome with the effectiveness of 98.21% precision, Recall of 96.89%, IOU of 93.93% and 98.36% F1-Score.

Keywords: *CNN Component filter, Gradients, Feature variable, Recursive filter and GNR Detector*

1. Introduction

The methane gas is a significant component of the planet's atmosphere and is one of the main causes for worldwide environmental degradation, known to be Greenhouse gas, it is about 86 times that is as of carbon dioxide [1]. As survey paper approached ch4 accounts about 20% among the other gases in the Global Warming [2]. JPL data set using AVIRIS-NG to collect, monitor such methane plume emissions. AVIRIS-NG [19] collects and record the information regarding the spectral wavelength range from visible to the spectral short Infra ranges available among the atmospheric levels. In the present work produced regarding the algorithms [5] that detected the methane plume signals from the AVIRIS-NG images which are about collected data of ch4 is almost about in the small signal range that is 2100nm to 2400nm. However the segmentation outcome from the algorithms can still be with the noisy signals within the retrieved outcome data. This work made to consider about combining the hybrid techniques which is about conventional and machine learning processing systems together.

The existing and present methods addresses the limitations about the system complexity and speed and Manual processing to be taken into the constellation because of day bottle line at retrieving the special information specially to detect and segment the plumes data over terrain data. Aerial images are commonly used to detect the sources of the plumes of the gases [4,5,6,7] and here it is methane and specifying its region and quantifying its area among the distributed terrain data. AVIRIS-NG are not meant or designed for detecting the gases but made to capture everyday spectral ranges in the atmospheric layers. Methaneand its plumes are identified and segmented using the wavelength range between 2215nm and 2410nm. The centric matching filter algorithm [7] found the presence of Methane Gas and its quantification which is commonly gathered by the average injections which are produced with the noising outcome along the false positive of the plumes present.

A significant impediment to the advancement of CH4 detection strategies is the restricted accessibility of public training data. A fresh dataset called Methane Hot Spots (MHS) has been released for machine vision. A unique one-step end-to-end method for hyperspectral transformer-based methane plume detection. In combination, both modules—spectral refiner[SFGQR]—enable localization of possible CH_4 plumes in the hyperspectral images using a Spectral-known linear extractor and enhance the query depiction for more effective decoding. This is an improvement over the conventional transformer design [3]. By carefully selecting associated pixels in the spectrum domain, a novel spectrum Linear Filter (SLF) enhances the performance of conventional linear filters by improving background distribution and enhancing methane signal.

Neighboring signal units or image pixels show a certain amount of similarity since their physical sources are uniform. Instead of using the conventional brute force methods, which grow exponentially with the number of

[1] *Visvesvaraya Technological University, India*
ORCID ID : 0009-0000-0822-2706
[2] *Visvesvaraya Technological University, India*
ORCID ID : 0000-0001-5152-0952
** Corresponding Author Email: snehavenkateshalu@gmail.com*

data, we can instead use contextual information in the form of features that characterize the studied signals or images. Our objective then shifts to find for certain confined characteristics in the data. Working in the feature space as opposed to the raw pixels has the additional benefit of solving the significant issue of pattern location changes in the data resulting from translation. Specifically, a feature-wise technique searches for particular forms anywhere in the signal, but a pixel-wise approach assumes a complete shift in pixels whenever a particular data feature changes its position.

In particular, the convolution window also known as the convolution filter or convolution kernel used in CNNs may identify just one feature that matches its shape. To achieve this, we apply feature matching across the entire signal, acting as if it were an analytical filter looking for particular shapes. Hyperspectral image can still be directly examine in terms of reality as indicated by the Einstein's berg colour notion. In another way, the reflecting properties of the context will be connected to the reduced image of dimensional pixels. Additionally, a built around off-the-shelf CNN may effectively minimise distortion from hyperspectral imaging with complement filter.

2. Related Work:

All printed material, the morphological patterns (MPs) suggested classifying data from remote sensing more accurately. MPs are created utilizing attributes that hold most of the data's information, including the PCA-derived elements. A new unsupervised approach called unpredictable PCA (NLPCA) auto-associative neural network was developed to condense the semantic depth of hyperspectral data with a small number of elements. Enhanced MPs constructed using NPCA characteristics to achieve precise classification. Linear correlations between spectral bands can be found using linear approaches. However, NLPCA finds combined linear as well as nonlinear relationships. The information content is spread proportionally throughout each element of NLPCA [25].

A statistical approach for discriminating between signals called Independent part discriminant Analysis (ICDA) used to satellite imagery categorization is centred on the adaptation of a Bayesian categorization rule to a signal made up of Independent Components (ICs). The converted elements are independently attributed to the Independent component analysis (ICA) transform array when information is transferred onto a separate space, making computation of the multimodal volume value as the sum of the unitary values simpler. After computing the weighting values for every independent element using a nonparametric kernel density estimator, the categorization allocation was made using the Bayes rule. Multiple hyperspectral pictures were subjected to the ICDA approach evaluation using support vector machines to examine multiple data set parameters, including urban/rural area, amount of the learning set, and kind [26].

With actual information in the structure of labelled data is often scarce, statistical categorization hyperspectral data is large in dimensionality, and reflect multiple categories of data that are occasionally extremely mixed together. The classification algorithms that are produced have a low generalization. Whenever analysing hyperspectral data, random forest types of filters inside a binary hierarchical multi-classifier framework enhance classifier generalization, particularly if the amount of learning data is constrained. Using spectral patterns that are spatially unstable to reflect random feature subset selection techniques' effectiveness concerning generalisation might be useful [27]. The kernels of the methods described for pattern analysis are computationally effective, robust, and reliable. For the classification of remotely sensed data, kernel-based classifiers have been developed and applied. Nonparametric ranked feature extraction (NWFE), which is based on a linear transformation, is employed to derive hyperspectral imagery attributes. The kernel approach is utilized to broaden the nonlinear and linear transformation of the NWFE to the kernel-based NWFE in the case of linear and nonlinear transformation. KNWFE will carry out Generalised Discriminant Analysis, Independent Factor Assessment, Core Based Primary Factor Analysis, and Resolution limits Feature Retrieval. This strategy lessens the impact of the kernel matrix's singularity on the resolution of eigenvalues [28].

The present machine learning analysis or algorithm methods are completely focus don't classify with the small portion targeted to detect among HSI imaging [12]. For such Logistic regressions are basically applied to retrieve the land covered among the raster HSI data employing point feature wise segmentation [11]. Multi labelling logistic regressions [13] are approaches which are directly focused on the class distributions this may cause to false positives [14]. Even built-in SVM kind decision for analysing but decision boundary with hard margins where may causethe miss classification, further effect the maximum margin classification among the classes [15, 16]. This method of hard margin classification causes the miss classification in large number which has its limitations at the underlining background distribution. Gaussian models produce the density of the data points with addition of its density is along with its mean and standard deviations this clustering kind of mixture model connect the components to classify the HSI raster data to varied terrain areas [17].

Hidden linear transforms performed to find the hidden data. One of the common analysis for HSI imaging is PCA. PCA gathers classes into set of axis that are uncorrelated.

This is largely used as one of the fast pre-processing step considered in the analysis [8, 9, 10]. One among the supervised learning technique is known to be ensemble learning for merging the multiple classifier predictors to get exactness in the outcome. Convolving PCA to reduce the curse of dimensionality which is followed in the depth learning data point methods made a solution to the chose decided area recognition. Further authors [29] in approached a 3D CNN connected end to end, get the predicted outcome among varied classes from the raster HSI data.

3. Proposed Approach

An off-the-shelf CNN approach

CNN picks up its weights on its own. In order to construct a neural network, the process of convolution can always add more than one convolution layer. The initial layer is in charge of acquiring gradients, while the subsequent layer is in charge of acquiring edges. The number of layers added dependent upon the parameter details of an image. Maintaining the initial dimensions of an object while using padding whose values rely on filters visual. The process of convolution layers, composed of a number of filters known as convolutional kernels, are a kind of neural network used by CNNs. Usually, convolutional filtering methods are employed over multiple levels, with the goal of identifying distinct features within an image. Convolutional networks enable fast and effective analysis and classification of impulses and images by acquiring many forms of the spectrum of features.

3.1 Component filter

Component filter is the linear filter chosen from MATLAB toolbox which produces the output values of linear combination pixels using convolution with time t. These filters said to be optimal filter as of their design based on optimization hypothesis required to minimize the error between a measured signal and an output signal. This is the linear time-unvarying hypothesis applied in image classification to preserve the signals / pixels of the input to refine the incoming data in the existence of supplement imaginary noise. The filter constituted employing the equation 1as shown in Fig.1

$x(t) = s(t) + w(t)$ (1) where $0 <= t <= T$

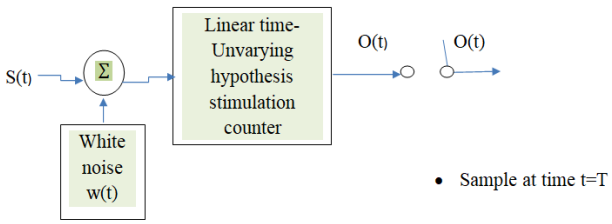

Fig.1. Component filter

The filter input x(t) include a transient signal s(t) altered by supplement mode noise w(t) with T as unpredictable observation interim. Transient signal s(t) representing as a 1/0 binary token. The mapping of w(t) is a noise operation with zero mean and spectral power density No/2. The changing signal s(t) detected optimally by the input signal x(t) by mapping with receiver. Since the hypothesis is linear, the resulting output o(t) may as below in eq.2

$$o(t) = s_0(t) + n(t) \quad (2)$$

The noise components of the input x(t) produces $s_0(t)$ and n(t) signals. In particular, the convolution window also known as a convolution filter or convolution kernel used in CNNs is able to identify approximately one feature that corresponds to its form. To achieve this, the component matching technique across the entire signal, acting as if it were analytical filters looking for methane shapes. For convolution kernel layer the equation represented as in eq.3

$$y(t) = (s*w)\ t \quad (3)$$

3.2 CNN approach for efficient classification

Conventional neural networks are the result of simplifying the CNN's input-output relationship as in Fig.2 with considering the element-wise form of the producing outcome layer offered by

$$y(t) = \sum_{k=1}^{T} s_k w_k(t) \quad (4)$$

Taking into account of component filter o(t) from eq.2 combining with convolutional kernel layers, where $w_k(t)$ classify the input to the neuron ‘k’ in a time instant ‘t’ produces as

$$y(t) = \sum_{k=1}^{T-1} s_k w_k(t) * o(t) \quad (5)$$

In the CNN one signal w(t) is considered as the input, when T samples of a signal appear at T input neurons simultaneously, it is referred to as w(t), and these are regarded as a single training datum. In the first convolutional layer, this data is linked to K outcome neurons, resulting in the input-output relationship inside the CNN architecture becoming

$$y_k = \sum_{m=0}^{T-1} s_k^1(m) w(m) * \sum_{t=\infty}^{T-1} o(t) \quad (6)$$

Applying element wise operation accounting ‘n’ input size with ‘m’ filter considering in kernel layer, the constant bias term appended to generate

$$y_k^1(n) = \sum_{m=0}^{M-1}(s_k^1(m)w(n+m) + b_k^1) * \sum_{t=\infty}^{T-1} o(t) \quad (7)$$

The overall amount of variables in each iteration is subsequently boosted by one to produce the following vector kind, which is the CNN outcome.

$$y_k^1 = x *_c (s_k^1 + b_k^1) * o(t) \quad (8)$$

The size of the feature matching (convolutional) filter is the only factor that determines how many weights (parameters) a CNN has with K convolution layer and M convolution filter.

The aggregate amount of weights for time-domain data, including the bias term, is K(M + 1). The total number of weights for a single image is K(M^2 + 1). In certain instances, the convergence phase outcome ought to match the dimensions of the input signal (picture), rather than the combination's minimum of (N − M + 1).If the input signal (picture) is padded 0.5 containing the right range of 0.5, this can be accomplished. For instance, we could add a 0.5 at for M = 3 and any value of N.

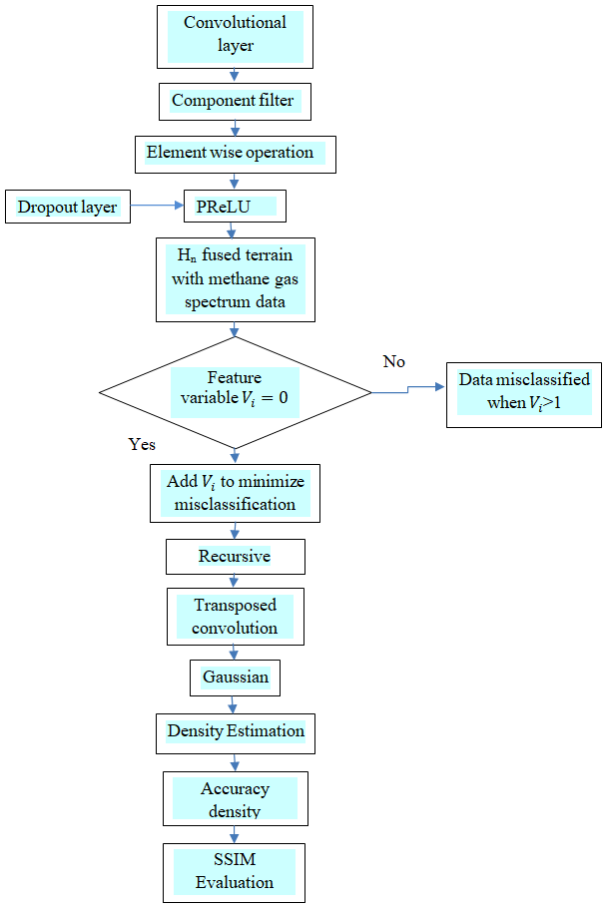

Fig.2. Off-the-shelf CNN

To compute the convergence product y(n), take x(−1) = 0.5 and add a zero at x(N) = 0.5 with component filter as represented in eq.9

$$y_k^1(n) = s_k^1(0.5)w(n-1) * o(t_1) + s_k^1(1.5)w(n) * o(t_2) + s_k^1(2.5)w(n+1)\ o(t_3) \quad (9)$$

Although convolution, or correlation, is a continuous functioning, signals and images are not at all like that. To do this, a convolutional layer's product is subjected to a non-linear behavior. A rectified linear unit (ReLU), defined by, is one of the most often used nonlinear activation function for CNNs.

$$f(x) = \max\{0, x\} \quad (10)$$

Gradients ultimately stops training, with cause of a unstable weights that gets saturate of data points in neural network. Effecting ReLU completely in dead state of neurons in a built model. To overcome function drawback, PReLU taken into picture that solve the problem of saturating andstopping the learning model when there is not their to learn for the model further, this is the generalized function of ReLU activation function. PReLU function learns the parameters adaptively of the rectifiers and improves accuracy [30].

$$f(x_i) = \begin{cases} x_i, & if\ x_i > 0 \\ a_i x_{i_i}, & if\ x_i \le 0 \end{cases} \quad (11)$$

Optimization [30] is achieved with PReLU while learning, employing the back propagation to optimize at the same time as well with other layers of network. The a_i updating as been done with applying chain rule, for one layer the gradient of a_i is:

$$\frac{\partial \varepsilon}{\partial a_i} = \sum_{x_i} \frac{\partial \varepsilon}{\partial f(x_i)} \frac{\partial f(x_i)}{\partial a_i} \quad (12)$$

Where ε is the optimization factor. The $\frac{\partial \varepsilon}{\partial f(x_i)}$gradient is of the depth layer in neural network. The activation function gradient is as followed

$$\frac{\partial f(x_i)}{\partial a_i} = \begin{cases} 0, & if\ x_i > 0 \\ x_i, & if\ x_i \le 0 \end{cases} \quad (13)$$

3.3 Methane gas segmentation from HSI raster data

The CNN approach allows labelling of the spectrum bands which is similar to the notion of Einstein's berg color. P is the array of pixels, A and B are the depth of terrain and gas spectrum data. H_n is originally a HSI raster data with subspace array of bands including 'i' gas spectrum length as represented in eq.14. Considering the curse of dimensionality, compressing of bands is required for the further processing of feature extraction of bands with respective to the reflecting properties of gas and as well the terrain data properties. At beginning the component filter applied for minimizing distortion from hyper spectral imaging of raster data as in eq.1,2.

$$\widetilde{H}_n = \frac{\sum_{o=1}^{A_n} H_n^p + \sum_{o=1}^{B_n} H_n^p}{A_n + B_n} \qquad (14)$$

The misclassification of gas spectrum among the terrain data is specified using the feature variable V_i and data considered to be incorrectly classified when $V_i > 1$, added feature variable to the layer when $V_i = 0$ as represented below

$$x_i(W_i^T V_i(X) + b) \geq \quad 1 - V_i \qquad (15)$$

To estimate the density of the data set H at point x is defined as followed

$$f(x,H) = \frac{1}{n} \cdot \sum_{x_i \in H} K_i(x - X_i) \qquad (16)$$

$$K_i(x - X_i) is the gaussian kernel function$$

The value of the density $f(x,H)$ differs from $f(x,H_i)$ because of the difference in distributions of the kind classes. Equivalently, the accuracy of the density $A(x,C_i,H)$ for the class C_i defined as followed

$$A(x,C_i,H) = \frac{n_i \cdot f(x,H_i)}{\sum_{i=1}^{k} n_i \cdot f(x,H_i)} \qquad (17)$$

4. Experimental Outcomes and Analysis

4.1 Dataset description

The data is pre-processed on a machine with Processor Intel(R) Xeon(R) Gold 5122 CPU @ 3.60GHz 3.59 GHz (2 processors), installed 64.0 GB RAM. The size of each image in H dataset is around 1.2 GB, and it takes time about 45 min to process each of the 46 data points in the dataset. The CNN used Component filters, Recursive filters with transposed convolution and Gaussian to get advanced evaluation computations of spectroscopic raster data.

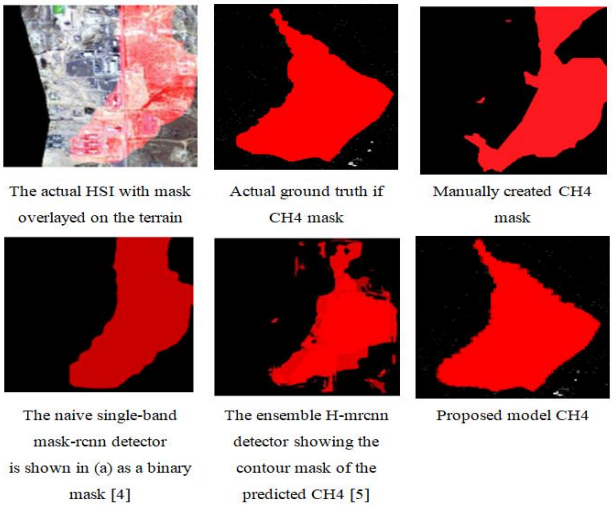

Fig.3 Segmentation of methane CH4

An experienced analyst examines every CH4 flightline, manually outlines plumes, and isolates features from any non-plume finds to create the ground truth data file. The manual method works well but is not scalable since it has major performance limitations related to computing time and human work hours. Further, the methane i.e., CH4 gas have been identified from the dataset collected from [6].

Table 1. Comparative Study with Outcome

Method	Precision	Recall	IOU	F1-score
Segment everything [4]	80	55	48	65
H-MRCNN [5]	96	91	87	94
Proposed	98.21	96.89	93.93	98.36

Evaluating gas localization:

Intersection over union: size of gas(plume data) / size of terrain data

4.2 Experimental Setup, Design and Results

The size of the convolution kernel is 128×1×40×40 with other convolution filter layers is 128×64×40×40. Applying softmax function with hyperparameters: Batch-size: 128, Dropout rate: 0.5, Learning rate: 1e-3, Batch normalization: 1e-5, Soft-max loss: 1e-6 and train Method = 'average'.

Recursive filter

Read N

N = number of iterations;

F = I_Par1;

```
sigma_H = sigma_s;
for i = 0:num_iterations – 1
sigma_H_i = sigma_H * sqrt(3) * 2^(N - (i + 1)) / sqrt(4^N - 1);
F = Transformed _Domain_Recursive_Filter_Horizontal(F, dHdx, sigma_H_i);
F = image_transpose(F);
F = Transformed_Domain_Recursive_Filter_Horizontal(F, dVdy, sigma_H_i);
F = image_transpose(F);
end
F = cast(F, class(img));
end
```

GNRs Detector

Snippet Functions of the Detector

```
% Read raw data
[D,info]=enviread([datapath],[datapath '.hdr']);
wl = sscanf(info.wavelength(2:end-1),'%f,');

% Vignetting correction, used for display and for adaptive thresholding
DfixVignett = vignettCorrection(D,info, dVignetting);

% Create mean intensity image, for display
meanI = repmat(mean(DfixVignett,3),[1 1 3]);
if scaleSeparate
   meanIScaled = equalizeRGBandUint3(meanI,0.01,0.02);
else % scale all channels together
   meanIScaled = equalizeRGBandUint(meanI,0.01,0.02);
end
% Create hyperspectral color image, for display
imgRGB = equalizeRGBandUint3(convert2RGB(DfixVignett,adjustable_bands,[80 80 80]),0.01,0.02);
figure; imshow(imgRGB);
% imwrite(uint8(imgRGB),[datapath '_hsi.png'])

% Pre processing
[Dp, location, aboveGnrThr] = prepData(D, info, cutoff, normEnable, gnrThr, noiseThr, smoothParams);
pixAboveNoise = length(aboveGnrThr);
pixAboveGnrThr = sum(aboveGnrThr);
locationAboveGnrThr = location(aboveGnrThr==1,:);

% Classification of each pixel above the threshold
% and show segmentation map
clusterNum = size(C,1);
label = zeros(length(Dp),1);
segmentationMap = zeros(size(D,1),size(D,2));
for ind = 1:length(location)
   if aboveGnrThr(ind)

% find nearest cluster center
      [~, I] = min(diag((repmat(Dp(ind,:),[clusterNum,1]) - C)*(repmat(Dp(ind,:),[clusterNum,1]) - C)'));
      label(ind) = I;
      if I == indCluster segmentationMap(location(ind,1),location(ind,2)) = 3; % nanoparticle
      elsesegmentationMap(location(ind,1),location(ind,2)) = 2; % tissue (high intensity)
      end
   else
segmentationMap(location(ind,1),location(ind,2)) = 1; % tissue (lower intensity)
   end
% 0 - background, the cover glass
end
figure; imagesc(segmentationMap); axis image; title('Threshold and detection map'); colormap jet; caxis([0 3]);
% saveas(gca,[datapath '_map.png'])
 pixGnr = sum(label==indCluster);
% number of detected pixels
imgOverlay = double(meanIScaled).*repmat((segmentationMap~=3),[1 1 3]) + repmat(permute(255*overlayColor,[3,1,2]),[size(meanIScaled,1) size(meanIScaled,2) 1]).*repmat(segmentationMap==3,[1 1 3]);
```

figure; imshow(uint8(imgOverlay));

title(['Pixels with label=' num2str(indCluster) ', mask'])

% imwrite(uint8(imgOverlay),[datapath '_detection_noiseThr=' num2str(noiseThr) '_gnrThr=' num2str(gnrThr) '.png'])

4.3 Estimation of SSIM for methane gas plumes segmentation analysis

Calculation of PSNRSSIM where Gaussian to carry out sophisticated spectroscopic data calculations:

psnr_cur=10*log10(255^2/mse);

mse_cur = mse/100;

window = fspecial('gaussian', 11, 1.5);

K(1) = 0.01;

K(2) = 0.03;

L = 255;

window = window/sum(sum(window));

sigma12 = filter2(window, img1.*img2, 'valid') - mu1_mu2;

ssim_map(index)=(numerator1(index).*numerator2(index)).(denominator1(index).*denominator2(index));

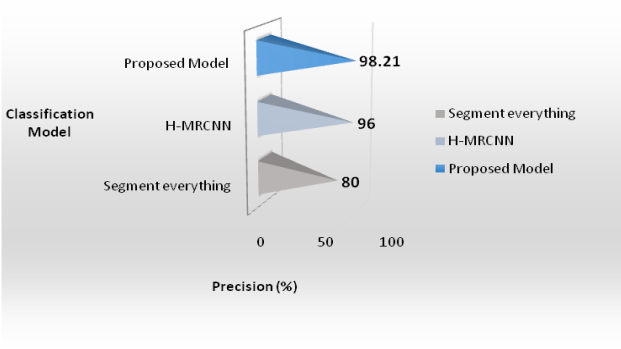

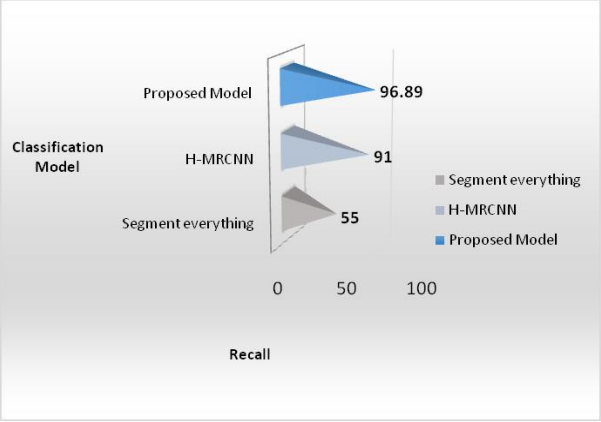

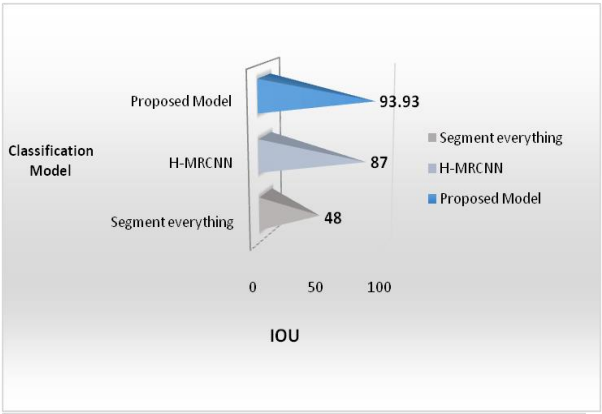

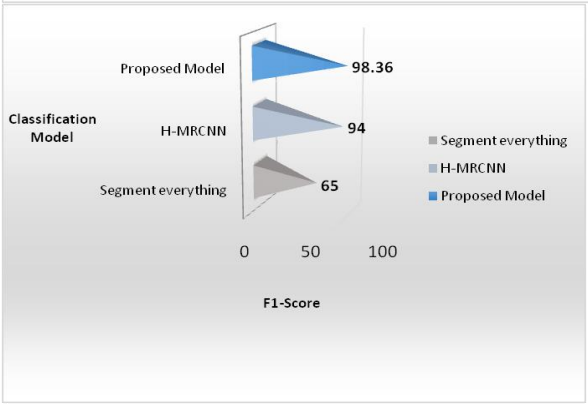

Fig.4: Methane plumes classification models among terrain HSI raster data

5. Conclusion

The available approaches couldn't provide effective outcome in shorter period. The off-the-shelf CNN based GNRs detectors to segment plumes effectively among the terrain HSI data, with tuning the hyperparameters in best possible manner to obtain the less misclassification of methane plumes over terrain data. Further for improving the classification feature variable is adopted to produce regularized outcome. The improved detector and optimized CNN gradients with component filter processed large hyperspectral imaging raster data. The processed data produced accurate outcome using the softmax loss aggregation of the convolutional filters, detectors and the features trained by varied layer stages, employment of transposed convolution over convolution increased the plumes spatial resolution of feature mapping. The max pooling applied for classifing the features specified to learn required class vectors, in faster prediction and classifying the labeled features utilize the PReLU activation function for further depth classification. Finally obtained the optimal convergence product, the off-the-shelf CNN using feature variable could improve the accuracy of segmenting plumes over terrain HSI raster data.

Acknowledgments

I always love to be gratitude towards my supreme, parents. I thank my supervisior for facilitating the system and tools to carry out my analysis in shorter period.

Author contributions

Sneha Venkateshalu: Conceptualization, Methodology, Software, Validation, Formal Analysis, Investigation, Data Curation, Writing—Original Draft Preparation, Writing—Review And Editing, Visualization, Project Administration; **Santhosh Laxman Deshpande:** Supervision**.**

Conflicts of Interest

The authors declare no conflict of interest.

References

[1] T.F. Stocker, D. Qin, G. K. Plattner, M. Tignor, S. K. Allen, J. Boschung, and P.M. Midgley, "The climate change 2013: The physical science basis", Working Group I contribution to the Fifth assessment report of the Intergovernmental Panel on Climate Change, Cambridge University Press, Cambridge, United Kingdom and New York, pp. 1585, 2014.

[2] S. Kirschke, P. Bousquet, P. Ciais, M. Saunois, J. G. Canadell, E. J. Dlugokencky, P. Bergamaschi, D. Bergmann, D. R. Blake, L. Bruhwiler, "Three decades of global methane sources and sinks", Nature geoscience, Vol. 6, No. 10, pp. 813-823, 2013.

[3] C. Frankenberg, U. Platt, and T. Wagner,"Iterative maximum a posteriori (IMAP)-DOAS for retrieval of strongly absorbing trace gases: Model studies for ch_4 and co_2retrieval from near infrared spectra of SCIAMQACHYonboardENVISAT", Atmospheric Chemistry and Physics, Vol. 5, No. 1, pp. 9-22, 2005.

[4] C. Frankenberg, A. K. Thorpe, D. R. Thompson, G. Hulley, E. A. Kort, N. Vance, J. Borchardt, T. Krings, K. Gerilowski, C. Sweeney, and et al.,"Airborne methane remote measurements reveal heavy-tail flux distribution in four corners region", Proceedings of the national academy of sciences, Vol. 113, No. 35, pp. 9734-9739, 2016.

[5] D. Thompson, I. Leifer, H. Bovensmann, M. Eastwood, M. Fladeland, C. Frankenberg, K. Gerilowski, R. Green, S. Kratwurst, T. Krings, and et al.,"Real-time remote detection and measurement for airborne imaging spectroscopy: a case study with methane", Atmospheric Measurement Techniques, Vol. 8, No. 10, pp. 4383-4397, 2015.

[6] A. K. Thorpe, C. Frankenberg, D. R. Thompson, R. M. Duren, A. D. Aubrey, B. D. Bue, R. O. Green, K. Gerilowski, T. Krings, J. Borchardt, and et al.,"Airborne DOAS retrievals of methane, carbon dioxide, and water vapor concentrations at high spatial resolution: application to AVIRIS-NG", Atmospheric Measurement Techniques, Vol. 10, No. 10, pp. 3833-3850, 2017.

[7] A. K. Thorpe, D. A. Roberts, E. S. Bradley, C. C. Funk, P. E. Dennison, and I. Leifer,"High resolution mapping of methane emissions from marine and terrestrial sources using a clustertuned matched filter technique and imaging spectrometry", Remote Sensing of Environment, Vol. 134, pp. 305–318, 2013.

[8] Y. Chen, X. Zhao, and X. Jia,"Spectral–spatial classification of hyperspectral data based on deep belief network", IEEE Journal of Selected Topics in Applied Earth Observations and Remote Sensing, Vol. 8, No. 6, pp. 2381–2392, 2015.

[9] S. T. Monteiro, Y. Minekawa, Y. Kosugi, T. Akazawa, and K. Oda,"Prediction of sweetness and amino acid content in soybean crops from hyperspectral imagery", ISPRS Journal of Photogrammetry and Remote Sensing, Vol. 62, No. 1, pp. 2-12, 2007.

[10] J. Xia, P. Du, X. He, and J. Chanussot,"Hyperspectral remote sensing image classification based on rotation forest. IEEE Geoscience and Remote Sensing Letters", Vol. 11, No. 1, pp. 239-243, 2013.

[11] Q. Cheng, P. K. Varshney, and M. K. Arora,"Logistic regression for feature selection and soft classification of remote sensing data", IEEE Geoscience and Remote Sensing Letters, Vol. 3, No. 4, pp. 491-494, 2006.

[12] U. B. Gewali, S. T. Monteiro, and E. Saber,"Machine learning based hyperspectral image analysis: a survey", Computer vision and pattern recognition, 2018.

[13] M. Khodadadzadeh, J. Li, A. Plaza, and J. M. Bioucas-Dias,"A subspace-based multinomial logistic regression for hyperspectral image classification", IEEE Geoscience and Remote Sensing Letters, Vol. 11, No. 12, pp. 2105-2109, 2014.

[14] S. Kumar, C. Torres, O. Ulutan, A. Ayasse, D. Roberts, and B. S. Manjunath, "Deep Remote Sensing Methods for Methane Detection in Overhead Hyperspectral Imagery", In: Proc. of IEEE Winter Conf. on Applications of Computer Vision (WACV), pp.1776-1785, 2020.

[15] D. M. Tax and R. P. Duin,"Support vector data description", Machine learning, Vol. 54, No. 1, pp. 45-66, 2004.

[16] W. Sakla, A. Chan, J. Ji, and A. Sakla. Ansvdd-based algorithm for target detection in hyperspectral imagery. IEEE Geoscience and Remote Sensing Letters, 8(2):384– 388, 2010.

[17] C. A. Shah, P. K. Varshney, and M. K. Arora, "ICA mixture model algorithm for unsupervised classification of remote sensing imagery", International Journal of Remote Sensing, Vol. 28, No. 8, pp.1711-1731, 2007.

[18] K. He, G. Gkioxari, P. Dollar, and R. Girshick. Mask r-cnn. ´ In Proceedings of the IEEE international

conference on computer vision, pages 2961–2969, 2017.

[19] L. Hamlin, R. O. Green, P. Mouroulis, M. Eastwood, D. Wilson, M. Dudik, and C. Paine,"Imaging spectrometer science measurements for terrestrial ecology: AVIRIS and new developments", In 2011 Aerospace conference, pp. 1-7, 2011.

[20] R. O. Duda, P. E. Hart, D. G. Stork, John Wiley & Sons, "Pattern Classification", 2000.

[21] S. Prasad, L. M. Bruce, "Limitations of principal components analysis for hyperspectral target recognition", IEEE Geoscience and Remote Sensing Letters, Vol. 5, No. 4, pp. 625–629, 2008.

[22] A. M. Martinez, A. C. Kak, "PCA versus LDA", IEEE Transactions on Pattern Analysis and Machine Intelligence, Vol. 23, No. 2, pp. 228-233, 2001.

[23] W. Li, S. Prasad, J. E. Fowler, and L. M. Bruce, "Locality-preserving dimensionality reduction and classification for hyperspectral image analysis", IEEE Transactions on Geoscience and Remote Sensing, Vol. 50, No. 4, pp. 1185-1198, 2012.

[24] F. Wu, Z. Wang, Z. Zhang, Y. Yang, J. Luo, W. Zhu, and Y. Zhuang, "Weakly Semi-Supervised Deep Learning for Multi-Label Image Annotation", IEEE Transactions on Big Data, Vol. 1, No. 3, pp. 109-122, 2015.

[25] G. Licciardi, P. R. Marpu, J. Chanussot, J. A. Benediktsson, "Linear versus nonlinear PCA for the classification of hyperspectral data based on the extended morphological profiles", IEEE Geoscience and Remote Sensing Letters, Vol. 9, No. 3, pp. 447-451, 2012.

[26] A. Villa, J. A.Benediktsson, J. Chanussot, and C. Jutten, "Hyperspectral image classification with Independent component discriminant analysis", IEEE Transactions on Geoscience and Remote Sensing, Vol. 49, No. 12, pp. 4865-4876, 2011.

[27] J. S. Ham, Y. Chen, M. M. Crawford, and J. Ghosh, "Investigation of the random forest framework for classification of hyperspectral data", IEEE Transactions on Geoscience and Remote Sensing, Vol. 43, No. 3, pp. 492-501, 2005.

[28] B. Schölkopf and A. J. Smola, "Learning with Kernels", The MIT Press, 2018.

[29] Y. Chen, H. Jiang, C. Li, X. Jia, and P. Ghamisi,"Deep feature extraction and classification of hyperspectral images based on convolutional neural networks", IEEE Transactions on Geoscience and Remote Sensing, Vol. 54, No. 10, pp. 6232-6251, 2016.

[30] S. Venkateshalu and S. Deshpande, "Performance Optimization of Short Video Using Convolutional Neural Network for IOT Applications", In: Proc. of the International conference on Paradigms of Communication, Computing and Data Sciences. Algorithms for Intelligent Systems. Springer, Singapore, pp. 743-754, 2022.